Micromechanics of MnAs nanocrystals embedded in GaAs

M. Moreno,[1,*] V. M. Kaganer,[2] B. Jenichen,[2] A. Trampert,[2] L. Däweritz,[2] and K. H. Ploog[2]
[1]*Instituto de Ciencia de Materiales de Madrid (CSIC), Cantoblanco, E-28049 Madrid, Spain*
[2]*Paul-Drude-Institut für Festkörperelektronik, Hausvogteiplatz 5-7, D-10117 Berlin, Germany*
(Received 21 June 2005; revised manuscript received 26 July 2005; published 15 September 2005)

The full strain state at room temperature of MnAs nanocrystals embedded in a GaAs matrix (GaAs:MnAs) is obtained through x-ray diffraction mapping of the GaAs:MnAs reciprocal space, including x-ray reflections from the nanosized MnAs crystallites. The constrained MnAs clusters are found to hold remarkably large and anisotropic strain. Based on the room-temperature experimental results, Eshelby's "equivalent-inclusion" concept is used to predict the thermal variation of the cluster lattice parameters in the temperature range from −50 up to 300 °C, in particular, across the MnAs magnetostructural phase transition. Strain-driven grain-boundary-mediated rotation and/or (imperfect) oriented attachment of MnAs clusters appear to be operative mechanisms of deformation and particle growth in granular GaAs:MnAs films.

DOI: 10.1103/PhysRevB.72.115206 PACS number(s): 75.50.Pp, 81.07.−b, 61.10.−i, 75.50.Tt

I. INTRODUCTION

Granular GaAs:MnAs, consisting of MnAs nanoclusters embedded in a GaAs matrix, is a promising hybrid ferromagnet-semiconductor material for novel information storage, magneto-optical, and spin electronics applications.[1–8] It can be synthesized by high-temperature annealing of diluted (Ga,Mn)As alloys grown by molecular-beam epitaxy (MBE) at low temperatures. Granular GaAs:MnAs exhibits several key properties: (i) excellent compatibility with III-V semiconductor technology, allowing overgrowth, (ii) ferromagnetism above room temperature due to the magnetic clusters, and (iii) feasibility of *n*-type doping of the matrix material surrounding the clusters.

The magnetic and structural properties of bulk MnAs are strongly coupled.[9–12] Residual strains in granular GaAs:MnAs, arising from the lattice mismatch between the MnAs clusters and the GaAs matrix, are likely to influence the magnetic properties of the material. Moreover, strain effects are expected to play an important role in the process of MnAs precipitation upon annealing (Ga,Mn)As. In order to understand the magnetic properties of GaAs:MnAs and to find out strategies to guide the assembly of the MnAs clusters within the GaAs matrix, it is crucial to know the strain state of the material. In this paper, we analyze the micromechanics of GaAs:MnAs epitaxial films on GaAs(001) substrates. Our analysis is based on x-ray diffraction (XRD) measurements of the interplanar distances in the MnAs nanocrystals at room temperature. We present reciprocal space maps of granular GaAs:MnAs films, including reflections from the MnAs crystallites. We use the Eshelby "equivalent-inclusion" concept[13–15] to predict the thermal variation of the MnAs-cluster lattice parameters.

II. EXPERIMENTAL DETAILS

Granular GaAs:MnAs films were synthesized by a high-temperature annealing of ternary $Ga_{1-x}Mn_xAs$ alloys grown by MBE at low temperature. We discuss results obtained for two samples, denoted S1 and S2. To synthesize sample S1 (S2), first a GaAs buffer layer was grown at 600 °C on a GaAs(001) substrate. The substrate was then cooled down to 300 °C (250 °C) for the growth of ~960 nm (~500 nm) of a ternary $Ga_{1-x}Mn_xAs$ alloy with $x \sim 0.06$. The $Ga_{1-x}Mn_xAs$ growth rate was 4 to 5 nm/min and the As_4/Ga beam-equivalent pressure ratio was 20–40. After growth, samples S1 and S2 were annealed *ex situ* in a rapid thermal annealing (RTA) oven under flowing nitrogen gas and covered with a GaAs wafer piece. In the RTA treatment, the samples were heated from 200 to 700 °C in 20 s, annealed at 700 °C for 20 s, and cooled down to 400 °C in 12 s. The annealing step gives rise to spherical hexagonal MnAs crystallites of variable diameter, in the range 20–45 nm, embedded in a GaAs matrix, as we observed in transmission-electron-microscopy (TEM) analysis. Samples S1 and S2 were seen to have essentially the same morphology. The samples may slightly differ in the Mn and/or As-excess contents. X-ray diffraction measurements were carried out in a PANalytical X'Pert diffractometer system, with a hybrid monochromator. A Ge triple-bounce analyzer crystal was used. The optimized optics provides a good resolution and a high intensity. It is well-suited for the study of nanosized particles, which show relatively broad diffraction maxima due to their small size. Two-dimensional maps over selected areas of the GaAs:MnAs reciprocal space were obtained by combining ω-2θ scans measured for different ω offsets.

III. X-RAY DIFFRACTION RESULTS

MnAs crystallites embedded in GaAs have been reported[1,16] to keep a well-defined orientation relationship ("nominal" orientation) with the GaAs matrix: the (00.1) basal planes of the MnAs crystallites are parallel to {111} GaAs planes, the ⟨01.0⟩ MnAs basal directions are parallel to $\langle 1\bar{1}2\rangle$ GaAs directions, and the ⟨11.0⟩ MnAs basal directions are parallel to $\langle 1\bar{1}0\rangle$ or ⟨110⟩ GaAs directions.[17] Four equivalent orientations of the MnAs clusters with respect to the GaAs matrix coexist, corresponding to MnAs (00.1) planes parallel to each of the four GaAs {111} plane orientations.

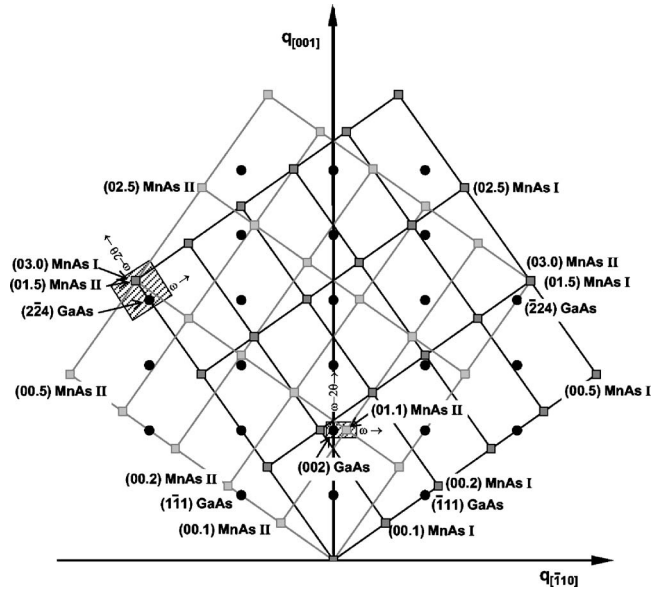

FIG. 1. Schematic view of the GaAs:MnAs reciprocal space across the plane containing the $q_{[001]}$ and $q_{[\bar{1}10]}$ GaAs scattering vectors. Dark circles correspond to Bragg spots of the GaAs matrix, dark-gray squares to Bragg spots of "type-I" MnAs clusters with basal planes parallel to ($\bar{1}$11) GaAs planes, and light-gray squares to Bragg spots of "type-II" MnAs clusters with basal planes parallel to (1$\bar{1}$1) GaAs planes. The probed regions are roughly marked as shaded areas, and the corresponding ω and ω-2θ directions are indicated.

The plane of the GaAs:MnAs reciprocal space that contains the [001] and [$\bar{1}$10] GaAs scattering vectors is sketched in Fig. 1, which shows only the Bragg spots corresponding to the GaAs matrix and to two, out of the four, MnAs-crystallite orientations: (i) MnAs clusters of "type-I" with (00.1) basal planes parallel to GaAs ($\bar{1}$11) planes, and (ii) MnAs clusters of "type-II" with (00.1) basal planes parallel to GaAs (1$\bar{1}$1) planes.[18] There are two additional sets of MnAs crystallites, "type-III" and "type-IV," with (00.1) basal planes parallel to

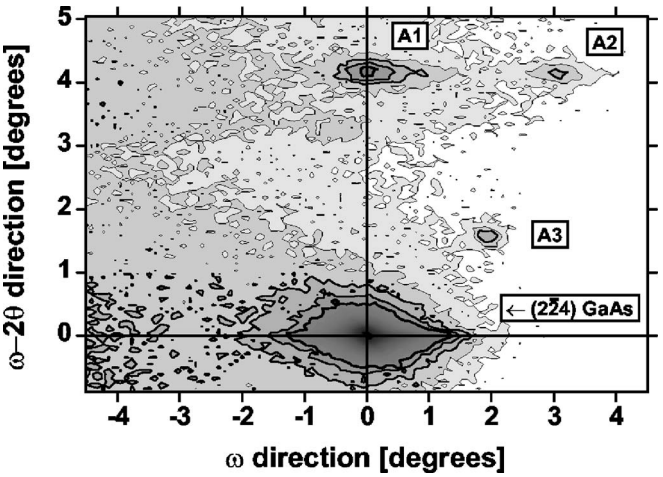

FIG. 2. Reciprocal-space map around the (2$\bar{2}$4) GaAs reflection of sample S1.

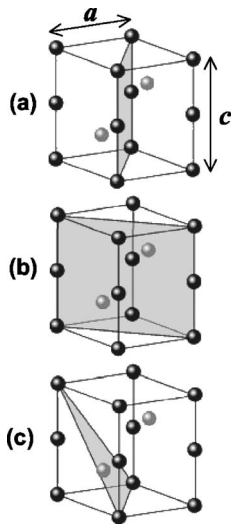

FIG. 3. Hexagonal unit cell of MnAs showing: (a) a (01.0) plane, (b) a (11.0) plane, and (c) a (01.1) plane.

GaAs (111) and ($\bar{1}\bar{1}$1) planes, respectively, but the diffracting plane of Fig. 1 is not a plane of high symmetry for these clusters. Figure 2 shows a reciprocal-space map of sample S1 around the GaAs (2$\bar{2}$4) substrate/matrix reflection, in the plane of Fig. 1. Besides the GaAs (2$\bar{2}$4) reflection, the map reveals three peaks. Peak A1 appears aligned with the (2$\bar{2}$4) GaAs reflection, and peaks A2 and A3 appear rotated towards increasing ω angles. According to the scheme of Fig. 1, we assign peak A1 to a superposition of diffraction intensities of the (03.0) and (01.5) reflections from type-I and type-II MnAs clusters, respectively. The good alignment—along the ω-2θ direction—of peak A1 with respect to the (2$\bar{2}$4) GaAs reflection indicates that the (01.0) planes of the MnAs crystallites are parallel to the (1$\bar{1}$2) planes of the GaAs matrix, as expected for MnAs crystallites with nominal orientation. Figure 3(a) shows a (01.0) plane within the MnAs unit cell.

The plane of the GaAs:MnAs reciprocal space that contains the [001] and [010] GaAs scattering vectors is sketched in Fig. 4, which shows only the Bragg spots corresponding to the GaAs matrix and to MnAs crystallites of "type-I" and "type-II." Figure 5 shows a reciprocal-space map of sample S1 around the (0$\bar{4}$4) GaAs reflection, in the plane of Fig. 4. A peak (B) appears aligned with the (0$\bar{4}$4) GaAs reflection. According to Fig. 4, we assign peak B to the (22.0) reflection from type-I MnAs clusters. The good alignment—along the ω-2θ direction—of peak B with respect to the (0$\bar{4}$4) GaAs reflection indicates that the (11.0) planes of the MnAs crystallites are parallel to the GaAs (0$\bar{1}$1) planes. Figure 3(b) shows a (11.0) plane within the MnAs unit cell.

We also probed a reciprocal-space region of sample S1 around the (002) GaAs reflection, in the plane of Fig. 1; this is shown in Fig. 6. Two peaks, C1 and C2, appear rotated towards positive ω values relative to the (002) GaAs reflection. According to Fig. 1, we assign peak C1 to the (01.1) reflection from type-II MnAs clusters. A MnAs (01.1) plane

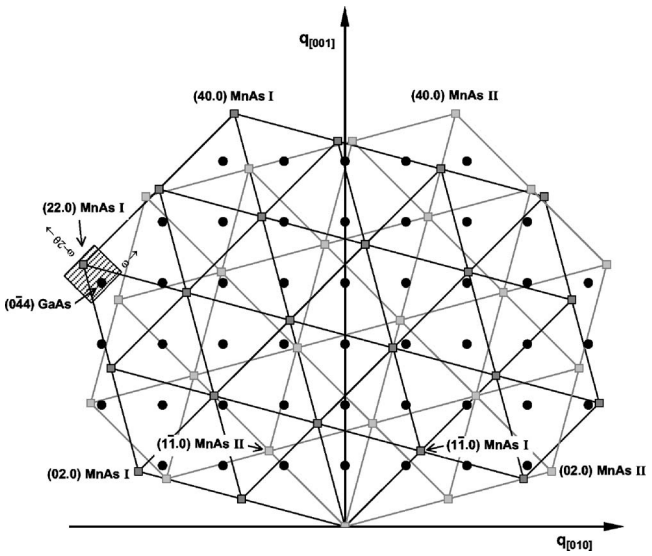

FIG. 4. Schematic view of the GaAs:MnAs reciprocal space across the plane containing the $q_{[001]}$ and $q_{[010]}$ GaAs scattering vectors. Dark circles, dark-gray squares, and light-gray squares correspond to Bragg spots of the GaAs matrix, of "type-I" MnAs clusters, and "type-II" MnAs clusters, respectively.

is shown in Fig. 3(c). Peak C2, in Fig. 6, appears about 3° rotated towards positive ω values with respect to C1. This is the same angle as the rotation of peak A2 with respect to peak A1 in Fig. 2. We assign peaks A2 and C2 to the (01.5) and (01.1) reflections, respectively, from MnAs clusters whose (00.1) basal planes are not exactly parallel to $(1\bar{1}1)$ GaAs planes but are about 3° rotated towards (001) GaAs around the [110] GaAs direction. The origin of peak A3 is unknown.

By recording low-noise ω-2θ and ω scans across the A1, B, and C1 diffraction peaks, we determined the interplanar spacings along three orthogonal directions of MnAs clusters

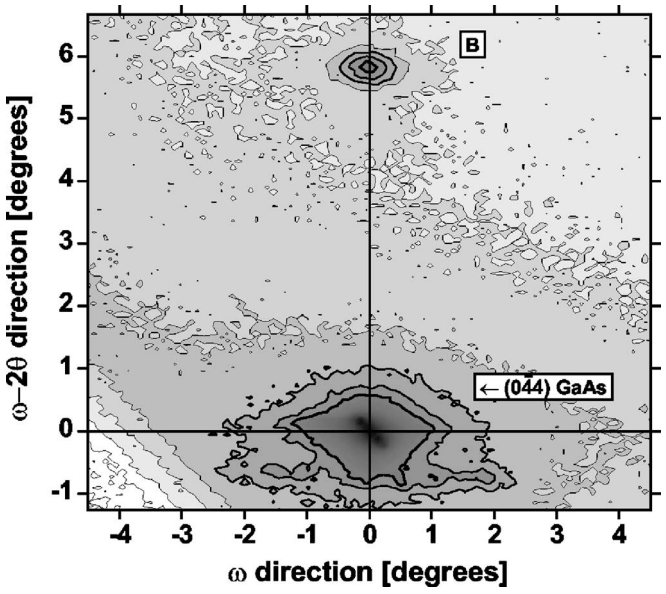

FIG. 5. Reciprocal-space map in the vicinity of the $(0\bar{4}4)$ GaAs reflection of sample S1.

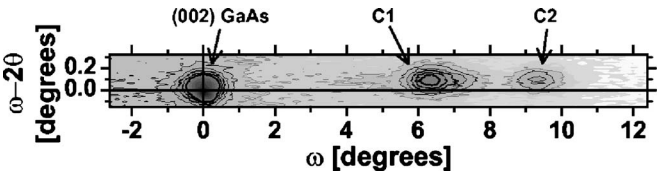

FIG. 6. Reciprocal-space map near the (002) GaAs reflection of sample S1.

with nominal orientation. The interplanar distance corresponding to a certain $\mathbf{q}$ reflection is given by $d=1/|\mathbf{q}|$. Here, $|\mathbf{q}|=[(q_\perp)^2+(q_\parallel)^2]^{1/2}$, where $q_\perp$ and $q_\parallel$ are the components of the scattering vector in the directions perpendicular and parallel to the plane of the film, respectively. The conversion of $(\omega,2\theta)$ coordinates into $(q_\perp,q_\parallel)$ coordinates is given by[19]

$$q_\perp = \frac{1}{\lambda}[\sin(2\theta-\omega)+\sin(\omega)],$$

$$q_\parallel = \frac{1}{\lambda}[\cos(2\theta-\omega)-\cos(\omega)], \quad (1)$$

where λ is the x-ray wavelength. Peak A1 gives the (01.0) interplanar distance $d_{(01.0)}=3.2113$ Å. The spacing is smaller than in unstrained bulk MnAs $d^{\text{bulk}}_{(01.0)}=3.2205$ Å.[20] The lattice of the MnAs crystallites is compressed by −0.29% in the [01.0] direction. Peak B gives the (11.0) interplanar distance $d_{(11.0)}=1.8538$ Å. The (11.0) interplanar distance in the MnAs crystallites is smaller than in unstrained bulk MnAs $d^{\text{bulk}}_{(11.0)}=1.8594$ Å.[20] The lattice of the MnAs crystallites is compressed by −0.30% in the [11.0] direction. Peak C1 gives the (01.1) interplanar distance $d_{(01.1)}=2.8112$ Å. The (00.1) interplanar spacing is then calculated from the already known (01.0) and (01.1) spacings. The obtained value, $d_{(00.1)}=5.8156$ Å, is notably larger than the spacing corresponding to bulk MnAs $d^{\text{bulk}}_{(00.1)}=5.7024$ Å.[20] The lattice of the MnAs clusters is expanded by as much as 1.99% along the c axis. The volume per Mn—As atomic pair ($V=\sqrt{3}a^2c/4$) in the MnAs crystallites is determined to be 34.63 Å^3, i.e., +1.4% larger than the volume corresponding to unstrained bulk MnAs (34.15 Å^3). On the other hand, from XRD measurements (not shown), the matrix of the granular GaAs:MnAs film was determined to be slightly tetragonally distorted, with a small in-plane tensile strain of $\Delta a/a=+0.021\%$.

In summary, the MnAs clusters are considerably distorted as compared to unstrained bulk MnAs. The approximately equal values of the strain along the [01.0] and [11.0] directions indicate that the MnAs-crystallite structure keeps hexagonal symmetry; no orthorhombic deformation occurs. The lattice largely expands along the c axis, and isotropically shrinks in the basal planes. Thus the elastic-strain tensor of the MnAs cluster at room temperature can be written as

TABLE I. Strain and stress in MnAs nanocrystallites embedded in a GaAs matrix at room temperature.

	Basal plane	c direction	Hydrostatic stress/ dilatation strain
Stress	+0.06 GPa	+2.13 GPa	+0.75 GPa
Elastic strain	−0.30%	+1.99%	+0.46%
Eigenstrain	+0.58%	−3.78%	−0.87%
Total strain	+0.28%	−1.79%	−0.41%

$$e_{ij} = \begin{pmatrix} e_a & 0 & 0 \\ 0 & e_a & 0 \\ 0 & 0 & e_c \end{pmatrix}, \tag{2}$$

where the x and y axes are two arbitrary orthogonal axes lying in the MnAs basal plane, and the z axis is parallel to the MnAs-crystallite c axis. Here,

$$e_a = \frac{a - a_b}{a_b}, \quad e_c = \frac{c - c_b}{c_b}, \tag{3}$$

where a and c are the lattice parameters of the constrained cluster at room temperature, and a_b and c_b are the equilibrium (unstrained) lattice parameters of bulk MnAs at room temperature. Elastic strains relate to stresses through the Hooke's law, $\sigma_{ij} = c^*_{ijkl} e_{kl}$. Here c^*_{ijkl} is the elastic-moduli tensor of the cluster (Ref. 21). The cluster elastic strains (obtained from the x-ray diffraction measurements), $e_a = -0.30\%$ and $e_c = +1.99\%$, relate to cluster stresses along the a and c axes $\sigma_a = +0.06$ GPa and $\sigma_c = +2.13$ GPa, respectively. The corresponding elastic dilatation $e_{\mathrm{dil}} = (2e_a + e_c)/3$ and hydrostatic stress $\sigma_{\mathrm{hyd}} = (2\sigma_a + \sigma_c)/3$ are given in Table I.

IV. THERMAL VARIATION OF THE CLUSTER STRAIN STATE

The strain in the MnAs clusters embedded in GaAs at room temperature originates from several sources. First, some strain builds up in the crystallites at the temperature of their formation (the *initial* strain) because of the mismatch of the MnAs and GaAs lattices. Further strain develops on cooling to room temperature (the *thermal* strain), due to the large difference between the thermal expansion coefficients of MnAs and GaAs. The lattice parameters of unstrained bulk MnAs crystals are known[9,22] in the temperature range from about −50 °C up to 300 °C, see Fig. 7. Bulk MnAs crystals have anomalously large thermal expansion coefficients of about 5×10^{-5} K^{-1} (Ref. 9), to be compared with the GaAs thermal expansion coefficient of 6×10^{-6} K^{-1} (Ref. 23). On cooling, the magnetostructural phase transformation of MnAs, at approximately 39 °C, gives rise to an abrupt increase of the lattice spacings in the basal plane by about 1% (the *phase-transformation* strain). At this phase transition, the nearest-neighbor distance in the basal plane increases abruptly and the nearest-neighbor distance along the c axis remains unchanged (see Fig. 7). Knowing the thermal variation of the lattice parameters of bulk MnAs material and the lattice parameters of the constrained MnAs cluster at room temperature, we determine below the thermal variation of the cluster lattice parameters.

Figure 8 shows projections of the GaAs and MnAs unit cells in the $[\bar{1}11]$-GaAs and [00.1]-MnAs directions (basal planes) and in the $[1\bar{1}2]$-GaAs and [01.0]-MnAs directions. The symmetries of the MnAs and GaAs basal planes are similar; the unit-cell size is slightly smaller in MnAs. The MnAs unit-cell length along the [00.1] direction is about 2/3 of the GaAs unit-cell length along the $[\bar{1}11]$ direction. In the granular GaAs:MnAs material, the MnAs cluster does not exactly replace a certain matrix volume. The replacement

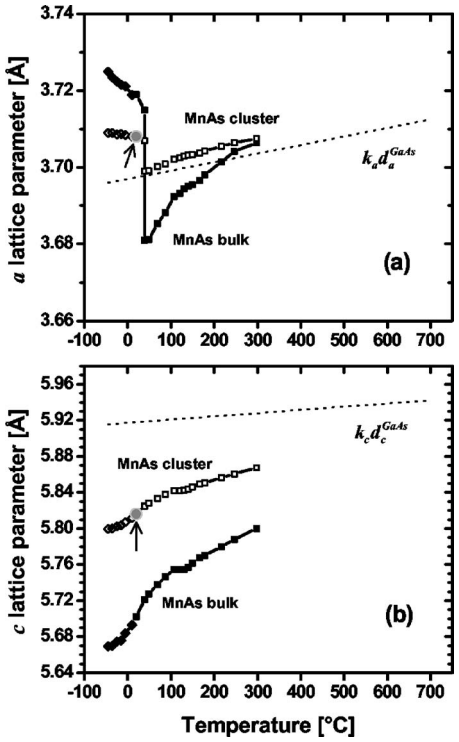

FIG. 7. Thermal variations of (a) the a lattice parameter, and (b) the c lattice parameter, for bulk MnAs crystals (closed symbols)—according to the experimental data reported by Willis and Rooksby (Ref. 9) (above 20 °C, closed squares) and by Govor (Ref. 22) (below 20 °C, closed diamonds)—and for MnAs nanoclusters embedded in a GaAs matrix (open symbols). The cluster room-temperature values (gray closed circles, marked by arrows) have been determined from XRD measurements and the thermal variation of the cluster structural parameters have been calculated. Dotted lines represent the GaAs-matrix length that a MnAs-cluster unit cell replaces in a and c directions.

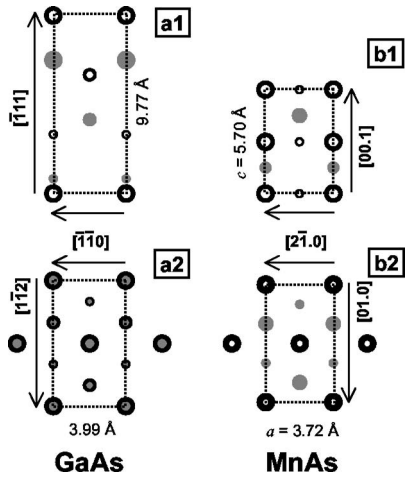

FIG. 8. Unit-cell symmetry and dimensions of unstrained bulk GaAs and MnAs crystals for two orthogonal projections (parallel to each other in GaAs:MnAs): (a1) GaAs $[1\bar{1}2]$, (a2) GaAs $[\bar{1}11]$, (b1) MnAs [01.0], and (b2) MnAs [00.1] directions. Gray-closed symbols represent As atoms and black-open symbols represent Ga or Mn atoms.

involves a volume mismatch. Therefore internal strains build up.

Description of the internal strains in granular GaAs:MnAs needs introduction of three different strain tensors.[13–15] The *total* cluster strain ε_{ij} is the expansion/contraction of the cluster when it is constrained by the matrix. The (proper) cluster *eigenstrain* ε_{ij}^p (also called stress-free transformation strain or self strain) is the expansion/contraction of the cluster when it is cut out of the matrix and allowed to expand or contract freely. Both the eigenstrain and the total strain are measured relative to the matrix volume that the cluster replaces. The difference between the total strain and the eigenstrain is the *elastic* strain $e_{ij}=\varepsilon_{ij}-\varepsilon_{ij}^p$. The elastic strain is the expansion/contraction of the constrained cluster relative to its equilibrium (free) volume. It is related to the stress by Hooke's law.

The cluster expansions/contractions represented by the total strain and eigenstrain are relative values, with a certain lattice frame as reference. Taking the bulk MnAs lattice at a temperature T_0 as the reference lattice, the eigenstrain components can be written as

$$\varepsilon_a^p(T)=\frac{a_b(T)-k_a d_a^{\mathrm{GaAs}}(T)}{a_b(T_0)},$$

$$\varepsilon_c^p(T)=\frac{c_b(T)-k_c d_c^{\mathrm{GaAs}}(T)}{c_b(T_0)}, \tag{4}$$

where $a_b(T)$ and $c_b(T)$ are the lattice parameters of the bulk MnAs crystal at the temperature T, while $d_a^{\mathrm{GaAs}}(T)$ and $d_c^{\mathrm{GaAs}}(T)$ are the sizes of the GaAs-matrix unit cell in a and c directions. The constants k_a and k_c are the number of GaAs-matrix lattice spacings that a MnAs-cluster lattice spacing replaces in a and c directions, respectively, at the reference temperature T_0. Hence the eigenstrain accounts for the mismatch between the volumes of the unstrained (free) cluster and matrix hole. Precipitation, thermal-expansion differences, and phase transitions can originate cluster-matrix volume mismatches and are thus sources of eigenstrain. The total-strain components can be written as

$$\varepsilon_a(T)=\frac{a(T)-k_a d_a^{\mathrm{GaAs}}(T)}{a_b(T_0)},$$

$$\varepsilon_c(T)=\frac{c(T)-k_c d_c^{\mathrm{GaAs}}(T)}{c_b(T_0)}, \tag{5}$$

where $a(T)$ and $c(T)$ are the lattice parameters of the constrained MnAs cluster at the temperature T. The total strain accounts for the mismatch between the volumes of the constrained cluster and matrix hole. Note that the definition of total strain involves the lattice spacings of the constrained cluster, while the definition of eigenstrain involves the lattice spacings of unstrained bulk material. The cluster elastic-strain components $e_{ij}=\varepsilon_{ij}-\varepsilon_{ij}^p$ are

$$e_a(T)=\frac{a(T)-a_b(T)}{a_b(T_0)}, \quad e_c(T)=\frac{c(T)-c_b(T)}{c_b(T_0)}. \tag{6}$$

The elastic strain is the deviation of the lattice spacing in the constrained cluster with respect to the lattice spacing in the unstrained bulk MnAs crystal at the same temperature T.

The eigenstrains at the temperature T can be decomposed in initial eigenstrains at the reference temperature T_0, $\varepsilon_a^p(T_0)$, and $\varepsilon_c^p(T_0)$, and (thermal) eigenstrain variations, $\Delta\varepsilon_a^p(T)$ and $\Delta\varepsilon_c^p(T)$:

$$\varepsilon_a^p(T)=\varepsilon_a^p(T_0)+\Delta\varepsilon_a^p(T), \quad \varepsilon_c^p(T)=\varepsilon_c^p(T_0)+\Delta\varepsilon_c^p(T), \tag{7}$$

where

$$\varepsilon_a^p(T_0)=\frac{a_b(T_0)-k_a d_a^{\mathrm{GaAs}}(T_0)}{a_b(T_0)}, \tag{8}$$

$$\varepsilon_c^p(T_0)=\frac{c_b(T_0)-k_c d_c^{\mathrm{GaAs}}(T_0)}{c_b(T_0)},$$

and

$$\Delta\varepsilon_a^p(T)=\frac{a_b(T)-a_b(T_0)}{a_b(T_0)}-\frac{k_a d_a^{\mathrm{GaAs}}(T_0)}{a_b(T_0)}\alpha(T-T_0),$$

$$\Delta\varepsilon_c^p(T)=\frac{c_b(T)-c_b(T_0)}{c_b(T_0)}-\frac{k_c d_c^{\mathrm{GaAs}}(T_0)}{c_b(T_0)}\alpha(T-T_0). \tag{9}$$

Here, we take into account that GaAs is a cubic crystal and its thermal expansion (α) is isotropic, so that

$$\frac{d_a^{\mathrm{GaAs}}(T)-d_a^{\mathrm{GaAs}}(T_0)}{d_a^{\mathrm{GaAs}}(T_0)}=\frac{d_c^{\mathrm{GaAs}}(T)-d_c^{\mathrm{GaAs}}(T_0)}{d_c^{\mathrm{GaAs}}(T_0)}=\alpha(T-T_0). \tag{10}$$

Similar decompositions in initial and thermal variation can be made for the total and elastic strains.

The problem of finding the relationship between the total strain and the eigenstrain (between the constrained and free expansions) was solved by Eshelby.[13,14] He showed that a

uniform eigenstrain in an inclusion of ellipsoidal shape gives rise to a uniform total strain in the inclusion. He obtained a tensor (the Eshelby tensor) S_{ijkl} relating these strains, $\varepsilon_{ij} = S_{ijkl}\varepsilon^p_{kl}$. This relationship is valid for the case of inclusion and matrix with equal elastic moduli (elastic homogeneity). Eshelby also extended this relationship to the case of different elastic moduli (elastic inhomogeneity). Let c_{ijkl} and c^*_{ijkl} be the elastic-moduli tensors of the matrix and inclusion, respectively. The stress in the inclusion

$$\sigma_{ij} = c^*_{ijkl}e_{kl} = c^*_{ijkl}(\varepsilon_{kl} - \varepsilon^p_{kl}) \tag{11}$$

can be expressed in terms of the matrix elastic moduli c_{ijkl} by introducing a *fictitious* eigenstrain ε^*_{ij} defined so that

$$c^*_{ijkl}(\varepsilon_{kl} - \varepsilon^p_{kl}) = c_{ijkl}(\varepsilon_{kl} - \varepsilon^p_{kl} - \varepsilon^*_{kl}). \tag{12}$$

Hence the Eshelby tensor S_{ijkl} relates the total strain ε_{kl} to the sum of the proper and fictitious eigenstrains $\varepsilon^p_{mn} + \varepsilon^*_{mn}$,

$$\varepsilon_{kl} = S_{klmn}(\varepsilon^p_{mn} + \varepsilon^*_{mn}). \tag{13}$$

If the eigenstrain ε^p_{kl} is known, the total strain ε_{kl} can be found by solving Eqs. (12) and (13).

Equations (12) and (13) can be solved in different approximations. The simplest approximation is assuming elastic isotropy and equal elastic moduli for the matrix and cluster (elastic homogeneity). The Eshelby tensor S_{ijkl} for spherical inclusions in an isotropic matrix[13–15] has the following nonzero components:

$$S_{1111} = \frac{7-5\nu}{15(1-\nu)},$$

$$S_{1122} = S_{1133} = \frac{5\nu-1}{15(1-\nu)}, \quad S_{1212} = \frac{4-5\nu}{15(1-\nu)}, \tag{14}$$

where ν is the Poisson ratio of the matrix. All other nonzero components are obtained by cyclic permutations of (1,2,3) or by the equivalency $S_{ijkl}=S_{jikl}=S_{ijlk}$. If the elastic moduli of the matrix and inclusion are taken equal to each other, the fictitious eigenstrain ε^*_{ij} is absent, Eqs. (12) are satisfied identically, and Eqs. (13) read

$$\varepsilon_a = \frac{1}{15(1-\nu)}[6\varepsilon^p_a + (5\nu-1)\varepsilon^p_c],$$

$$\varepsilon_c = \frac{1}{15(1-\nu)}[2(5\nu-1)\varepsilon^p_a + (7-5\nu)\varepsilon^p_c]. \tag{15}$$

We take the elastic constants of the MnAs cluster equal to those of the GaAs matrix (Ref. 24). To simulate elastic isotropy, we take the Poisson ratio resulting from a Voigt average of the GaAs elastic moduli. This gives the GaAs Poisson ratio $\nu=0.23$. Using this ν value, we obtain

$$\varepsilon_a = 0.519\varepsilon^p_a + 0.013\varepsilon^p_c,$$

$$\varepsilon_c = 0.026\varepsilon^p_a + 0.506\varepsilon^p_c. \tag{16}$$

In the case of different elastic moduli of the matrix and cluster we obtain, in the approximation of elastic isotropy, an analytical solution of Eqs. (12) and (13):

$$\varepsilon_a = \frac{2(4-5\nu)\mu^*}{6(4-5\nu)\mu^* + 3(7-5\nu)\mu}(\varepsilon^p_a - \varepsilon^p_c) + \frac{(1+\nu)K^*}{3(1+\nu)K^* + 6(1-2\nu)K}(2\varepsilon^p_a + \varepsilon^p_c),$$

$$\varepsilon_c = \frac{-4(4-5\nu)\mu^*}{6(4-5\nu)\mu^* + 3(7-5\nu)\mu}(\varepsilon^p_a - \varepsilon^p_c) + \frac{(1+\nu)K^*}{3(1+\nu)K^* + 6(1-2\nu)K}(2\varepsilon^p_a + \varepsilon^p_c), \tag{17}$$

where K, μ and K^*, μ^* are the compressibility and shear moduli of the matrix and cluster, respectively. The compressibility and shear moduli of the GaAs matrix and MnAs cluster obtained through a Voigt average are $K=75.4$, $\mu=48.7$, $K^*=27.3$, $\mu^*=27.6$ (in units of GPa). Using these values we obtain

$$\varepsilon_a = 0.313\varepsilon^p_a - 0.021\varepsilon^p_c,$$

$$\varepsilon_c = -0.043\varepsilon^p_a + 0.334\varepsilon^p_c. \tag{18}$$

Finally, in the general case of elastic anisotropy and different elastic moduli of the matrix and cluster, the Eshelby tensor S_{klmn} is expressed by integrals[15] that we calculated numerically. For MnAs clusters embedded in GaAs, we obtain

$$\varepsilon_a = 0.232\varepsilon^p_a - 0.039\varepsilon^p_c,$$

$$\varepsilon_c = 0.010\varepsilon^p_a + 0.473\varepsilon^p_c. \tag{19}$$

Note that the off-diagonal terms are small compared to the diagonal ones and that the cluster is elastically softer in the c direction than in the a direction. A comparison of the approximations (16) and (18) with the "exact" solution (19) shows the need of fully taking into account the elastic anisotropy and inhomogeneity of the GaAs:MnAs system in order to obtain correct total-strain values for given eigenstrains. Expressing the total strain in Eqs. (19) as the sum of the eigenstrain and elastic strain, the direct relationship between eigenstrain and elastic strain is obtained.

We take the room temperature as the reference temperature T_0, and the bulk MnAs lattice at room temperature as the reference lattice for the strains. First, knowing the room-temperature elastic strain (initial elastic strain), we determine—using Eqs. (19)—the cluster total strain and eigenstrain at room temperature (initial total strain and eigenstrain); the obtained values are listed in Table I. Then, knowing the initial eigenstrain, we determine—using Eqs. (8)—the number of GaAs-matrix unit cells that a MnAs-cluster unit cell replaces in a and c directions. We obtain $k_a=0.927$ and $k_c=0.606$. That is, 1000 MnAs unit cells replace 927 GaAs unit cells (about 1 MnAs unit cell replaces 1 GaAs unit cell, see Fig. 8) in the a direction, and 1000 MnAs

unit cells replace 606 GaAs unit cells (about 3 MnAs unit cells replace 2 GaAs unit cells, see Fig. 8) in the c direction. The replacement involves a lattice mismatch (initial eigenstrain) between cluster and matrix: the unstrained cluster (the free cluster outside of the matrix) is 0.58% larger in the a direction and 3.78% smaller in the c direction than the matrix hole. Finally, Eqs. (4), (5), and (19) can be used to express the lattice parameters of the constrained cluster, $a(T)$ and $c(T)$, as functions of the unstrained bulk lattice parameters, $a_b(T)$ and $c_b(T)$. We hence calculate the thermal variation of the cluster lattice parameters in the temperature range where the bulk lattice parameters are known, i.e., from about −50 °C up to 300 °C. The results are shown in Fig. 7.

V. DISCUSSION

The thermal variation of the lattice parameters is smaller for MnAs clusters embedded in GaAs than for bulk MnAs crystals because of the elastic constrain imposed by the GaAs matrix. Across the magnetostructural phase transition, the change of the a spacing in the cluster constrained by the matrix is predicted to be about 30% of the corresponding change in bulk MnAs [see Fig. 7(a)]. This prediction is in good agreement with the experimental results recently reported[25] by Couto *et al.* Their experiments have shown[25] the a-lattice-parameter change across the phase transition to be broad for constrained clusters, the transition extending over about 30 °C.

The strain in the MnAs cluster is predicted to decrease upon heating from room temperature. Along the a axis, the cluster strain appears to be zero or very small above 300 C [Fig. 7(a)]. However, along the c axis, the cluster strain is predicted to be still large (+1.18%) at 300 °C, and a linear extrapolation of the matrix and cluster lattice parameters up to 700 °C appears to indicate a strained state for the cluster at the annealing temperature [Fig. 7(b)]. This is relevant for cluster self-assembly strategies using strain effects.

The equilibrium volume per Mn—As atomic pair predicted[26] for the zinc-blende MnAs structure (in between 43.9 and 46.3 Å^3) is much larger than the room-temperature and 300 °C volumes (34.63 and 34.92 Å^3, respectively) obtained here for the MnAs crystallites embedded in GaAs. Hence the strain in the MnAs crystallites within the temperature range 20–300 °C is not large enough to drive a transition from the NiAs-type structure to the zinc-blende structure.

Here, we calculate the thermal variation of the cluster strain state assuming that the clusters are noninteractive. Interactions between clusters, i.e., effects of the surrounding clusters on the strain fields experienced by a given cluster, on the one hand, give rise to inhomogeneous strain fields within each cluster ("intracluster fluctuations"). On the other hand, they cause the levels of the average strains in individual clusters to differ ("intercluster fluctuations"). Such interaction effects can be accounted for via effective field theories (Mori-Tanaka methods). A refined calculation of this type is beyond the scope of the present work. The lattice parameter values here calculated can be regarded as average values for the clusters across the sample.

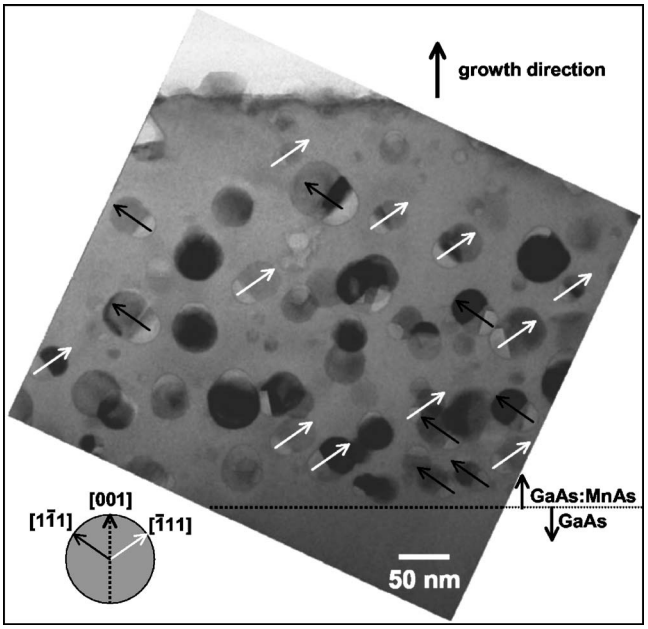

FIG. 9. Cross-sectional bright-field TEM image of sample S2. The arrows mark ⟨111⟩ GaAs directions, which are aligned with [00.1] MnAs directions of nominally oriented MnAs crystallites.

Deformation mechanisms in nanocrystalline materials can be quite different from deformation mechanisms taking place in infinite bulk materials. Grain boundary-mediated plasticity substitutes for conventional dislocation nucleation and motion as the dominant deformation mechanism when grain sizes are reduced below a certain value.[27–29] Grain rotation has been identified as a grain boundary-mediated deformation mechanism in nanocrystalline materials.[30–32] Moreover, (imperfect) oriented attachment[33,34] is an important mechanism by which nanoparticles coarsen. This mechanism may apply when particles nucleate side-by-side and coalesce during growth. Our x-ray-diffraction and transmission-electron-microscopy analyses of granular GaAs:MnAs films appear to indicate that strain-driven grain-boundary-mediated rotation and/or (imperfect) oriented attachment of MnAs nanocrystals occur during the synthesis of granular GaAs:MnAs. Figure 9 shows a cross-sectional bright-field TEM image of sample S2. MnAs particles are seen to agglomerate. Note that the interfaces between agglomerated MnAs particles are often nearly parallel to (00.1) MnAs planes, which are parallel to {111} GaAs planes. That is, the interfaces between agglomerated MnAs particles are often nearly perpendicular to the crystallite direction (c axis) that sustains higher strain. The extra x-ray diffraction peaks (A2, C2, A3) seen in the GaAs:MnAs reciprocal-space maps are likely associated to rotated MnAs particles, attached to nominally oriented MnAs particles.

VI. CONCLUSIONS

We have analyzed the micromechanics of granular GaAs:MnAs epitaxial films on GaAs(001) substrates. The full strain state of the MnAs nanoclusters at room temperature has been determined through x-ray diffraction analysis.

As compared to bulk MnAs, the lattice of the MnAs crystallites has been found to be isotropically compressed by −0.30% in the basal planes and largely expanded by +1.99% along the *c* axis. Deformation of the MnAs-cluster crystalline structure occurs with a net increase of the unit-cell volume of +1.4%. The large and anisotropic strain built up in the MnAs crystallites at room temperature appears to be due to (i) the elastically softer nature of MnAs as compared to GaAs, (ii) the anomalously large MnAs thermal expansion coefficients, and (iii) the change of the MnAs *a* lattice parameter across the first-order magnetostructural phase transition. In the constrained MnAs clusters, the magnetostructural phase transition is predicted to occur with smaller change of the *a* lattice parameter as compared to bulk MnAs. Deformation mechanisms typically found in bulk materials appear to be hindered in granular GaAs:MnAs. In contrast, strain-driven grain-boundary-mediated rotation and/or (imperfect) oriented attachment of MnAs clusters appear to be operative mechanisms of deformation and particle growth in granular GaAs:MnAs.

ACKNOWLEDGMENTS

This work has been partly supported by the German Federal Ministry for Education and Research, by the CSIC/European Social Fund through the I3P Program, by the European Commission through the Human Resources and Mobility activity under Contract No. MERG-CT-2004-6373, and by the Spanish Ministerio de Educación y Ciencia under Grant No. MAT 2004-5348.

*Email address: mmoreno@icmm.csic.es

[1] J. De Boeck, R. Oesterholt, A. Van Esch, H. Bender, C. Bruynseraede, C. Van Hoof, and G. Borghs, Appl. Phys. Lett. **68**, 2744 (1996).
[2] P. J. Wellmann, J. M. Garcia, J.-L. Feng, and P. M. Petroff, Appl. Phys. Lett. **71**, 2532 (1997).
[3] H. Akinaga, J. De Boeck, G. Borghs, S. Miyanishi, A. Asamitsu, W. Van Roy, Y. Tomioka, and L. H. Kuo, Appl. Phys. Lett. **72**, 3368 (1998).
[4] K. Ando, A. Chiba, and H. Tanoue, Appl. Phys. Lett. **73**, 387 (1998).
[5] P. J. Wellmann, J. M. Garcia, J.-L. Feng, and P. M. Petroff, Appl. Phys. Lett. **73**, 3291 (1998).
[6] H. Akinaga, S. Miyanishi, K. Tanaka, W. Van Roy, and K. Onodera, Appl. Phys. Lett. **76**, 97 (2000).
[7] H. Shimizu, M. Miyamura, and M. Tanaka, Appl. Phys. Lett. **78**, 1523 (2001).
[8] S. U. Yuldashev, Y. Shon, Y. H. Kwon, D. J. Fu, D. Y. Kim, H. J. Kim, T. W. Kang, and X. Fan, J. Appl. Phys. **90**, 3004 (2001).
[9] B. T. M. Willis and H. P. Rooksby, Proc. Phys. Soc. London, Sect. B **67**, 290 (1954).
[10] C. P. Bean and D. S. Rodbell, Phys. Rev. **126**, 104 (1962).
[11] R. H. Wilson and J. S. Kasper, Acta Crystallogr. **17**, 95 (1964).
[12] N. Menyuk, J. A. Kafalas, K. Dwight, and J. B. Goodenough, Phys. Rev. **177**, 942 (1969).
[13] J. D. Eshelby, Proc. R. Soc. London, Ser. A **241**, 376 (1957).
[14] J. D. Eshelby, Proc. R. Soc. London, Ser. A **252**, 561 (1959).
[15] T. Mura, *Micromechanics of Defects in Solids* (Martinus Nijhoff, Dordrecht, 1987).
[16] M. Moreno, A. Trampert, B. Jenichen, L. Däweritz, and K. H. Ploog, J. Appl. Phys. **92**, 4672 (2002).
[17] We use the (*hkil*) "four-indices notation" for the MnAs planes, omitting the third index $i=-(h+k)$.
[18] Figure 1 has been constructed using the unstrained bulk GaAs lattice parameter $a_b=5.65359$ Å and the unstrained bulk MnAs lattice parameters $a_b=3.7187$ Å and $c_b=5.7024$ Å reported by J. Mira, F. Rivadulla, J. Rivas, A. Fondado, T. Guidi, R. Caciuffo, F. Carsughi, P. G. Radaelli, and J. B. Goodenough, Phys. Rev. Lett. **90**, 097203 (2003).
[19] D. K. Bowen and B. K. Tanner, in *High Resolution X-ray Diffractometry and Topography* (Taylor & Francis, London, 1998), p. 149.
[20] The unstrained lattice parameter in a certain direction, d_b, is calculated using the bulk a_b and c_b lattice parameters reported by J. Mira, F. Rivadulla, J. Rivas, A. Fondado, T. Guidi, R. Caciuffo, F. Carsughi, P. G. Radaelli, and J. B. Goodenough, Phys. Rev. Lett. **90**, 097203 (2003).
[21] The elastic constants in Voigt notation of hexagonal MnAs are [M. Dörfler and K. Bärner, Phys. Status Solidi A **17**, 141 (1973)] $C^*_{11}=40$, $C^*_{12}=8$, $C^*_{13}=10$, $C^*_{33}=110$, and $C^*_{44}=34$ (in units of GPa).
[22] G. A. Govor, Sov. Phys. Solid State **23**, 841 (1981).
[23] *Landolt-Börnstein Tables*, edited by O. Madelung (Springer, Berlin, 1982), Vol. 17a.
[24] The elastic constants in Voigt notation of cubic GaAs are [H. J. McSkimin, A. Jayaraman, and P. Andreatch, Jr., J. Appl. Phys. **38**, 2362 (1967)] $C_{11}=118.77$, $C_{12}=53.72$, and $C_{44}=59.44$ (in units of GPa).
[25] O. D. D. Couto, Jr., M. J. S. P. Brasil, F. Iikawa, C. Giles, C. Adriano, J. R. R. Bortoleto, M. A. A. Pudenzi, H. R. Gutierrez, and I. Danilov, Appl. Phys. Lett. **86**, 071906 (2005).
[26] S. Sanvito and N. A. Hill, Phys. Rev. B **62**, 15553 (2000).
[27] S. Yip, Nature (London) **391**, 532 (1998).
[28] J. Schiotz, F. D. Di Tolla, and K. W. Jacobsen, Nature (London) **391**, 561 (1998).
[29] H. V. Swygenhoven, Science **296**, 66 (2002).
[30] K. E. Harris, V. V. Singh, and A. H. King, Acta Mater. **46**, 2623 (1998).
[31] D. Moldovan, D. Wolf, and S. R. Phillpot, Acta Mater. **49**, 3521 (2001).
[32] Z. Shan, E. A. Stach, J. M. K. Wiezorek, J. A. Knapp, D. M. Follstaedt, and S. X. Mao, Science **305**, 654 (2004).
[33] R. L. Penn and J. F. Banfield, Science **281**, 969 (1998).
[34] Z. Yu, M. A. Hahn, J. Calcines, T. D. Krauss, and J. Silcox, Appl. Phys. Lett. **86**, 013101 (2005).